



Article

# Viroporins of Mpox Virus

Kingshuk Basu , Miriam Krugliak and Isaiah T. Arkin \*

Department of Biological Chemistry, The Alexander Silberman Institute of Life Sciences,  
The Hebrew University of Jerusalem, Edmond J. Safra Campus, Jerusalem 91904, Israel;  
kingshuk.baso@mail.huji.ac.il (K.B.); miriamkru@savion.huji.ac.il (M.K.)

\* Correspondence: arkin@huji.ac.il

**Abstract:** Mpox or monkeypox virus (MPXV) belongs to the subclass of Poxviridae and has emerged recently as a global threat. With a limited number of anti-viral drugs available for this new virus species, it is challenging to thwart the illness it begets. Therefore, characterizing new drug targets in the virus may prove advantageous to curbing the disease. Since channels as a family are excellent drug targets, we have sought to identify viral ion channels for this virus, which are instrumental in formulating channel-blocking anti-viral drugs. Bioinformatics analyses yielded eight transmembranous proteins smaller or equal to 100 amino acids in length. Subsequently, three independent bacteria-based assays have pointed to five of the eight proteins that exhibit ion channel activity. Finally, we propose a tentative structure of four ion channels from their primary amino acid sequences, employing AlphaFold2 and molecular dynamic simulation methods. These results may represent the first steps in characterizing MPXV viroporins en route to developing blockers that inhibit their function.

**Keywords:** Mpox virus; viral ion channels; ion channel assay; molecular dynamic simulation



**Citation:** Basu, K.; Krugliak, M.; Arkin, I.T. Viroporins of Mpox Virus. *Int. J. Mol. Sci.* **2023**, *24*, 13828. <https://doi.org/10.3390/ijms241813828>

Academic Editors: Istvan Simon and Mario Milani

Received: 1 August 2023

Revised: 17 August 2023

Accepted: 4 September 2023

Published: 7 September 2023



**Copyright:** © 2023 by the authors. Licensee MDPI, Basel, Switzerland. This article is an open access article distributed under the terms and conditions of the Creative Commons Attribution (CC BY) license (<https://creativecommons.org/licenses/by/4.0/>).

## 1. Introduction

Among the recent outbreaks of different viral strains, Mpox or monkeypox is a potentially alarming disease. The scientific community is trying to gain insight into the epidemiology, dynamics of transmission and molecular characteristics of the virus responsible for the infection. Mpox virus, or MPXV, the etiological agent of Mpox, is a member of Poxviridae that emerged in 1958 among primates, and since 1970, it has been found to infect humans [1]. Though the disease was initially contained primarily within central and West African countries, after May 2022, several cases were found in European countries [2–4]. The symptoms of Mpox are similar but milder than smallpox, e.g., muscle aches, headache, fever, rash, and lymph node swelling [5], which is of no surprise since the coding regions of MPXV and variola virus, the etiological agent of smallpox, are over 96% identical [6]. Finally, Mpox is a zoonotic disease, but its animal reservoir is yet to be uncovered [7].

Despite a large number of studies, only two FDA-approved drugs are available in the market against Mpox: Tecovirimat [8,9] and Brincidofovir [10,11]. Both of these drugs are known to inhibit viral replication. Tecovirimat is known to target the VP37 protein, which assists in extracellular viral particle formation [9]. On the other hand, Brincidofovir targets the DNA polymerase enzyme, which aids viral DNA synthesis [11].

In addition to the above protein targets, viroporins as a family represent another attractive viral component to inhibit [12–15]. For example, the M2 H<sup>+</sup> channel of the Influenza A virus serves as the target of aminoadamantanes [16] that have been known to inhibit influenza since 1964 [17]. Consequently, research has been devoted to identifying and targeting viral ion channels, such as JC virus Agnoprotein [18–20], to increase the scope of anti-viral drugs [21–24].

MPXV is an oval-shaped virus with a length of 220–450 nm [25], larger than HIV or SARS-CoV-2 viruses [26]. Similarly, the double-stranded DNA genome size of MPXV of 197 kb [27] is significantly larger than the aforementioned two pathogens and is thought to

encode around 200 proteins [28]. However, to the best of our knowledge, viroporins have not been reported for the virus.

In the current study, we have employed a bacteria-based characterization of MPXV transmembrane proteins and analyzed their potential to function as ion channels. Following our experimental investigation, we made tentative structural predictions for the top-performing ion channels based on AlphaFold2 [29] and molecular dynamic simulations. These biochemical and structural characterizations can cast light on how to formulate future anti-viral drugs against this disease.

## 2. Results

### 2.1. Sequence Analysis

Ion channel proteins transverse through the lipid bilayer and, as such, are transmembrane in nature. Accordingly, we searched the 200 kb genome of MPXV [6] for proteins containing transmembrane segments with Phobius [30] and TMMHM [31]. Due to the large number of proteins identified and the overall small size of viroporins, we arbitrarily decided to limit our study to proteins equal to or smaller than 100 amino acids in length. With this criterion in hand, eight small transmembrane domains were chosen: C20.5L, A15.5L, gp124, gp063, gp066, gp125, gp081, and gp120. Their corresponding accession numbers, lengths, and probable TM domains are listed in Table 1, and their sequences are given in Supplementary Figure S1.

**Table 1.** List of transmembrane proteins chosen from MPXV genome with their accession numbers, length, and predicted transmembrane domains according to Phobius [30] and TMMHM [31].

Protein	Accession No.	Size	Predicted Transmembrane Domain
C20.5L	WBK62766.1	49	6–29 (according to Phobius) 5–23 (according to TMMHM)
A15.5L	WBK62635.1	53	7–24 and 30–50 (according to Phobius) 7–25 and 30–50 (according to TMMHM)
gp124	WBK62631.1	70	5–22 (according to Phobius) 4–24 (according to TMMHM)
gp063	WBK62763.1	73	45–69 (according to Phobius) 46–69 (according to TMMHM)
gp066	WBK62621.1	79	5–29 and 49–71 (according to Phobius) 7–29 and 49–72 (according to TMMHM)
gp125	WBK62620.1	90	10–33 and 46–67 (according to Phobius) 9–30 and 46–69 (according to TMMHM)
gp081	WBK62619.1	92	42–62 and 67–90 (according to Phobius) 40–60 and 67–90 (according to TMMHM)
gp120	WBK62749.1	100	45–68 (according to Phobius) 45–69 (according to TMMHM)

### 2.2. Experimental Channel Examination

#### 2.2.1. Expression and Membrane Incorporation of Proteins

As expounded below, we expressed the above-stated proteins in three bacterial systems suitable for investigating channel activity. These systems were used to analyze numerous viroporins and, as such, demonstrated their applicability and suitability [21–24,32–34].

#### 2.2.2. Negative Assay

In the negative assay, a viral protein is expressed at increasing levels, and if it exhibits channel activity, it causes commensurate permeabilization of the bacterial membrane. In other words, growth retardation is observed as a phenotypical expression of the channel [33]. This method is particularly helpful for checking the activity of viral channel blockers since they alleviate the growth impairment [21–24,32,33].

Figure 1 shows the growth rates of bacteria expressing the different aforementioned viral proteins. The growth was measured as a function of OD<sub>600nm</sub> with respect to time,

from which a maximal growth rate was determined. Upon increasing the concentration of the IPTG inducer, a corresponding reduction in growth rate is observed for the bacteria that express most chimeras, albeit at different levels. Specifically, at 60  $\mu\text{M}$  IPTG, bacteria that express gp120, C20.5L, gp081, A15.5L, gp063, gp125, gp066, and gp124, exhibited a relative growth reduction of: 31%, 38%, 42%, 54%, 75%, 77%, 97%, and 103%, respectively.

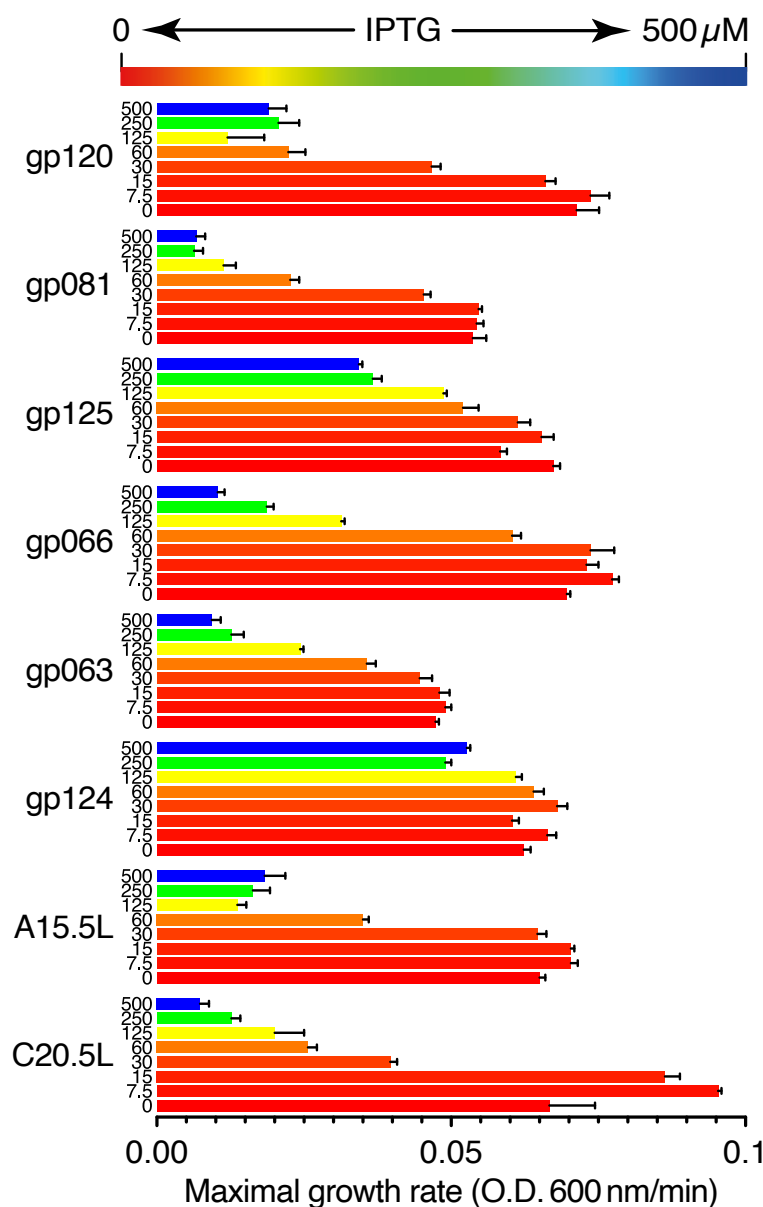


**Figure 1.** Negative genetic test for viroporin activity. The impact of expression of viral protein chimera upon bacterial growth, as a function of the concentration of protein inducer IPTG from 0 to 500  $\mu\text{M}$ .

### 2.2.3. Positive Assay

In the positive assay, a  $\text{K}^+$ -uptake deficient strain of bacteria is used in the analysis. The bacteria cannot grow in LB media unless it is supplemented by  $[\text{K}^+]$  or expresses a channel capable of  $\text{K}^+$  transport [35]. Hence, growth enhancement is observed as a phenotypical expression of the viral protein [36], which is reciprocal to the negative assay discussed above. Note that in this instance, the expression level of the channel is lower than in the negative assay to prevent deleterious excess membrane permeabilization [37].

Figure 2 depicts the effect of the expression of different viral proteins on cellular growth. Upon expression of gp120, A15.5L, gp081, C20.5L, and gp063 proteins, we observed a 208%,

221%, 101%, 82%, and 47% increase in bacterial growth in comparison to their uninduced forms, respectively. On the other hand, upon induction of gp125, gp066, and gp124, no significant change in bacterial growth rate was observed.

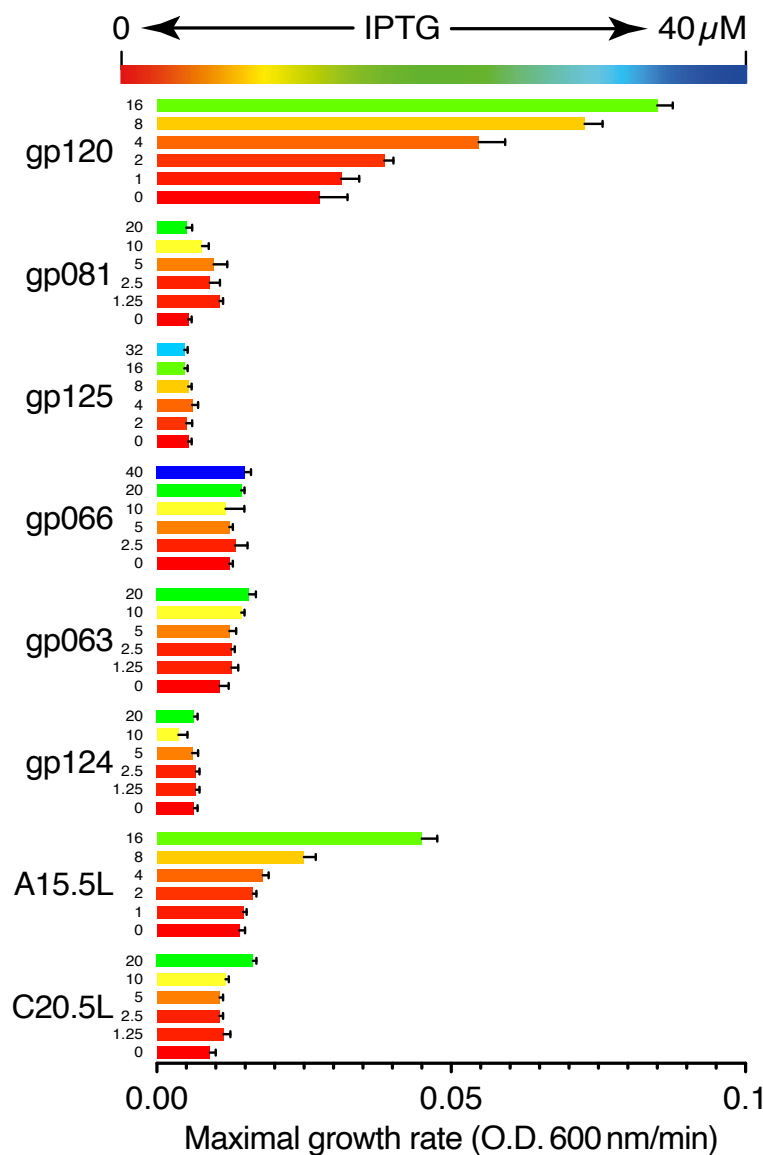


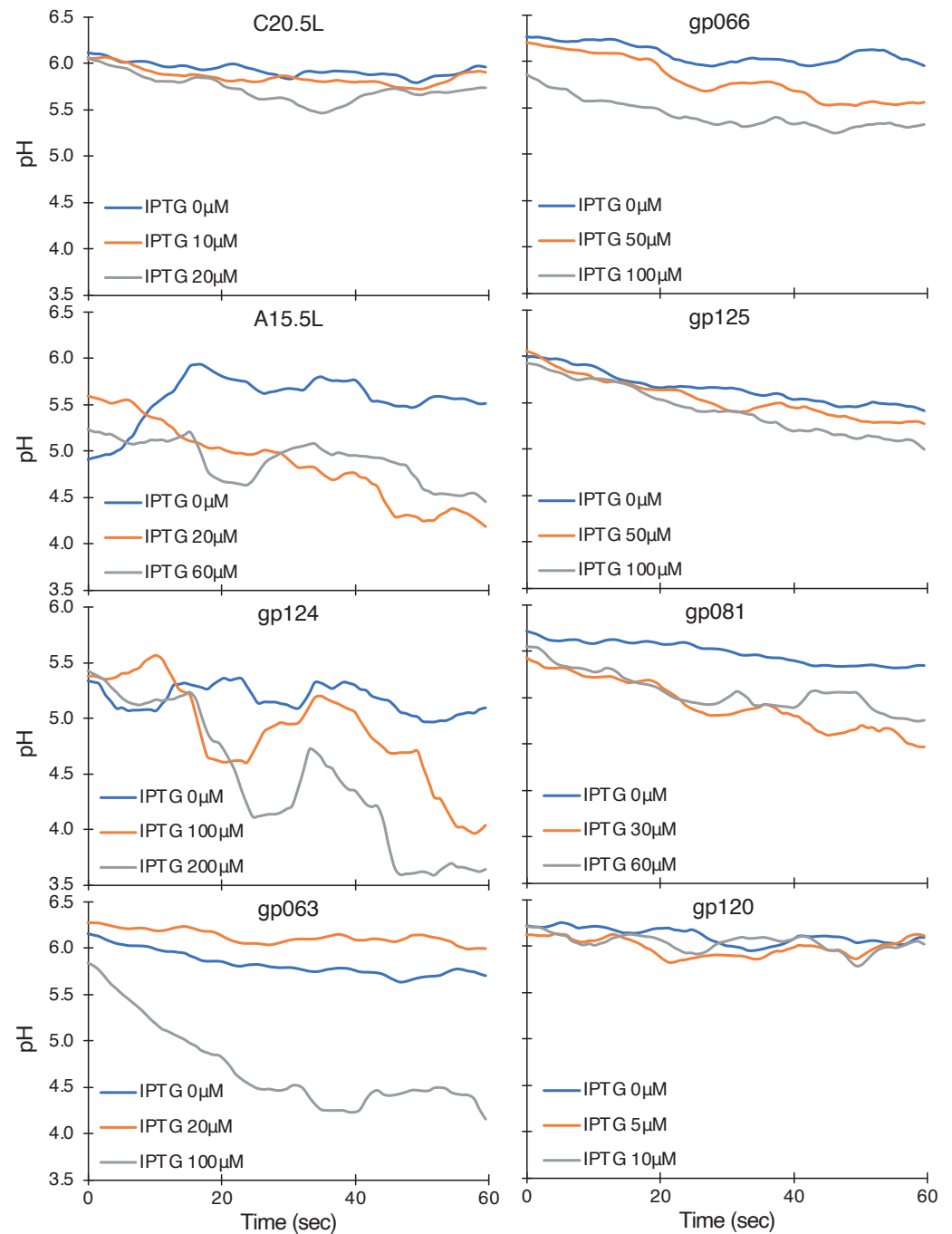
**Figure 2.** Positive genetic test for viroporin activity. The protein chimeras were expressed within a  $K^+$ -uptake deficient bacteria [35] to examine whether they trigger  $K^+$  flux and increase the growth rate of bacteria.

#### 2.2.4. pH Assay

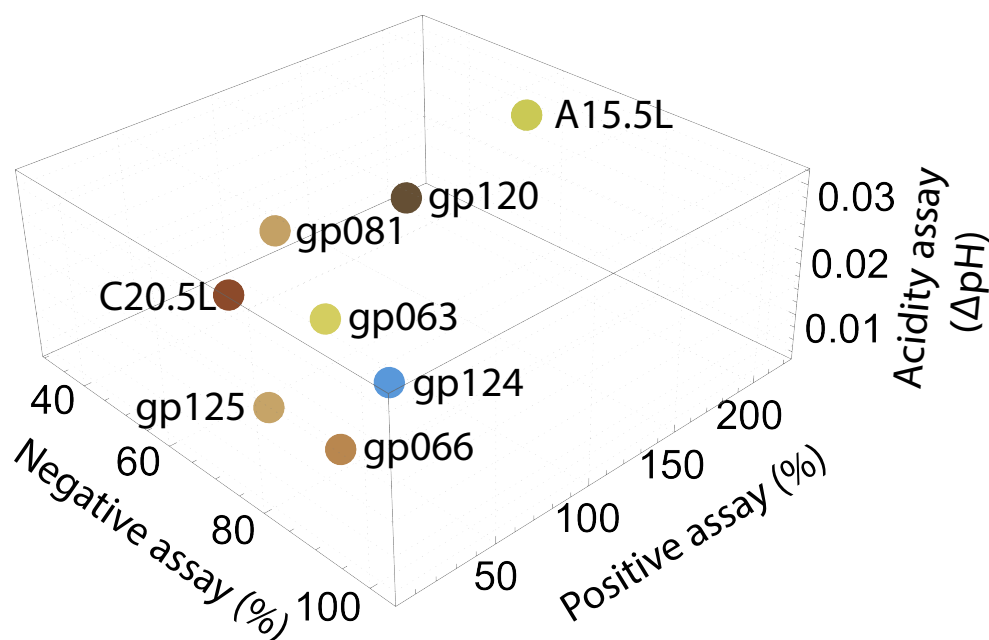
In the final experimental assay, the  $H^+$  intake kinetics of the bacterial cells were checked upon expression of the viral proteins. In this assay [34], a particular strain of bacteria expresses pHluorin, a pH-sensitive green fluorescent protein [38]. pHluorin has two excitation maxima at 390 nm and 460 nm, and the ratio between them is a function of the pH within the cell. Therefore, the activity of a protein capable of  $H^+$  transport can be detected by fluorescence upon injection of an acidic solution into the media.

Figure 3 shows the pattern of pH change in the bacterial cells upon expression of different proteins. Bacteria that express the gp124, A15.5L, gp063, gp125, gp081, and gp066 chimera exhibit a pronounced pH drop indicative of their  $H^+$  conductivity, while those expressing C20.5L and gp120 do not. The slopes of the linear regressions of the data are listed in Figure 4. Here, it is worth mentioning that the concentration of IPTG chosen for the

different proteins was not uniform. We only studied the maximal pH influx for a particular channel. Furthermore, another intermediate concentration of IPTG was selected to show an increment of pH influx upon increasing IPTG concentration.



**Figure 3.** Fluorescent-based  $H^+$  influx assay. The proton uptake was measured as function of fluorescence excitation peak maxima at 390 nm and 460 nm at several different protein induction levels governed by the IPTG concentration, as noted in the figure.



**Figure 4.** Diagram presenting a summary of the bacteria-based assay results for channel activity for the different viral proteins. The negative assay results represent the relative growth inhibition at 60  $\mu$ M IPTG (Figure 1). The positive assay results are taken from Figure 2. The pH assay results are obtained from the slopes of linear regressions of the results presented in Figure 3.

### 2.3. Computational Studies

The results of the negative assay (Figure 1), positive assay (Figure 2), and fluorescent-based  $H^+$  influx assay (Figure 3) are summarized as a 3D plot in Figure 4 and in tabulated form in Supplementary Table S1. Based on their effectivity in each assay, ranks were assigned, and based on averaged rank, five proteins that may serve as viroporins were selected for further computational studies: A15.5L, gp081, gp120, gp063, and C20.5L. We, therefore, proceeded to employ molecular modeling to obtain a primary insight into the ion channels' structural features. In brief, AlphaFold2 structural prediction yielded models for the proteins, followed by molecular dynamics simulation analyses of their structural integrity within a lipid bilayer.

#### 2.3.1. Structure Prediction

After the success of AlphaFold [29], AlphaFold2 (AF2 from Google CoLab [39]) has emerged as a more efficient tool for making structural predictions of proteins from their amino acid sequences. Moreover, AF2 has been found to predict the structures of trans-membrane proteins with higher accuracy than soluble proteins [40].

A key consideration in the modeling process was the oligomeric nature of the proteins. Due to their small size and channel activity, the proteins are most likely oligomeric, in line with other viroporins [41]. However, since the oligomeric number is unknown, we used AF2 to generate structures of differing oligomeric structures ranging from trimer to hexamer for each of the putative viroporins. Subsequently, two criteria were used to select the probable oligomeric number: (i) the presence of a pore throughout the structure since it is necessary for conduction, and (ii) the highest level of sequence-wise confidence score marked by the pLDDT score [42].

Supplementary Figure S2 shows the per-residue confidence estimates (pLDDT plots) obtained from AF2 for the different oligomeric structures. It can be concluded from the distribution of confidence levels that all protein sequences, except A15.5L, show the highest confidence level for their corresponding trimeric structure. A15.5L, on the other hand, shows the highest confidence level for a tetrameric structure. Finally, we did not obtain structures containing a lumen surrounded by a helical bundle for either oligomer of gp081.



Supplementary Figure S3 shows the top structures (rank one) chosen for further computational studies, obtained from AlphaFold2 with corresponding position-wise confidence value plots.

### 2.3.2. Molecular Dynamics Simulations

The structural models obtained from AF2 were subsequently analyzed by molecular dynamics simulations. The probable transmembrane region of each oligomer was inserted in a hydrated lipid bilayer and subjected to a 100 ns trajectory. The stability of the proteins was examined by measuring the RMSD values of the backbone for each simulation with respect to time, as shown in Figure 5. It is evident from the plots that every structure converges to stable conformers with relatively similar RMSD values at the higher time scale of each trajectory. Such stable structures with similar RMSD values for each protein were overlapped (approximately 70 structures for each protein) to yield a representative structure of the proteins within the lipid environment, as shown in Figure 6.

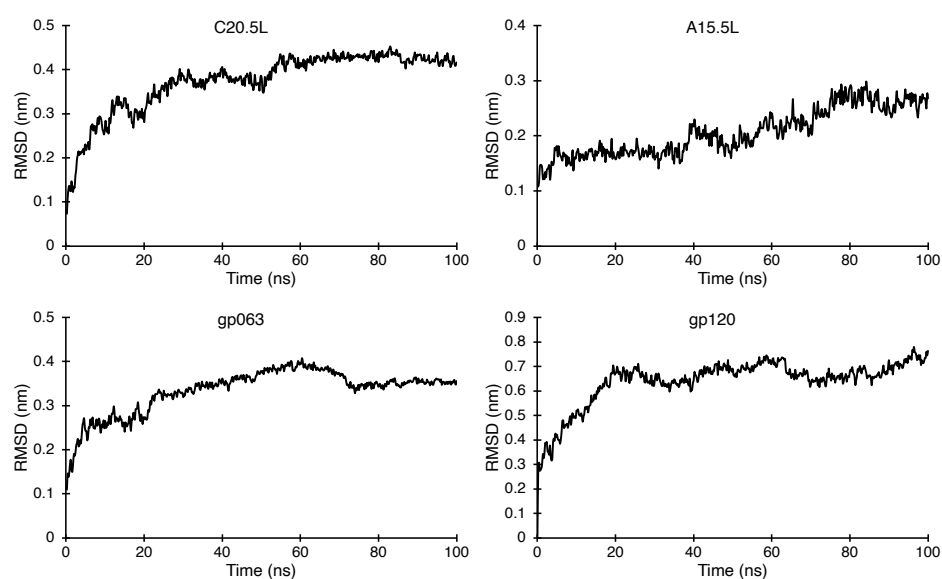


**Figure 5.** Backbone RMSD plots as a function of time for the molecular dynamics simulation of proteins: C20.5L, A15.5L, gp063, and gp120 within a pre-equilibrated 1,2-dipalmitoyl-sn-glycero-3-phosphocholine bilayer.

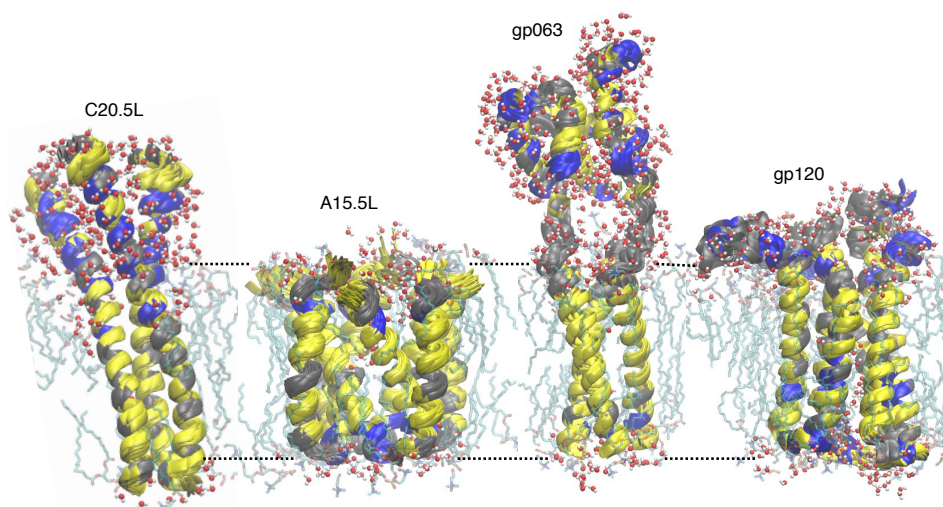


**Figure 6.** One hundred (100) ns MD simulated overlapped ensemble structures of C20.5L, A15.5L, gp063, and gp120 embedded within a triphasic lipid bilayer. Rough bilayer boundaries are shown in dotted lines with lipid and water molecules within 3 Å vicinity of proteins.

### 3. Discussion

The Mpox virus is an emerging threat to the healthcare sector, and options for medicinal remedies are wanting. Channels as a family are excellent drug targets, and by inference, viral ion channel blockers represent an attractive anti-viral strategy to inhibit viral infectivity. However, to achieve such an aim, we first need to identify potential viral ion channels in MPXV and characterize their activity. To achieve this goal, we employed three bacteria-based channel assays to evaluate the activity of putatively predicted ion channels from the corresponding protein sequences.

Ion channels are transmembranous in nature. Therefore, it is necessary first to identify proteins with one or more transmembrane domains to explore channels. From different sequence analysis techniques, we found the following MPXV proteins which have probable transmembrane domain(s): C20.5L, A15.5L, gp124, gp063, gp066, gp125, gp081, and gp120 (see Table 1 and Supplementary Figure S1, which includes the transmembrane domain lengths and positions). We studied the channel activity of these proteins using three different bacteria-based biochemical assays and proposed the probable structure of the effective ion channels using computational tools.

Bacterial channel assays are based on three different techniques used to quantify the activity of ion channels expressed in the organism's inner membrane. A phenotypic difference in the bacteria is obtained upon channel expression at varying levels in all three assays. Finally, reproducible membrane targeting and incorporation is achieved by fusing the viral proteins to the maltose binding protein [21–24,32–34].

The negative assay entails retarding the growth of the host bacteria upon increasing expression of viral ion channels due to membrane permeabilization (under the control of Isopropyl- $\beta$ -D-1-thiogalactopyranoside). We found a significant setback in bacterial growth upon increasing the expression of all the aforementioned proteins except for the gp124 chimera (Figure 1).

The positive assay does the opposite job of the negative assay. In a  $K^+$ -uptake deficient bacterial system, ion channel expression causes an increase in growth rate [35]. Interestingly, in this assay, we found pronounced ion channel activity effects for gp120, A15.5L, gp081, gp063, and C20.5L chimeras (Figure 2).

The third assay we employed measured quantitatively the kinetics of proton influx upon induction of the ion channels. For the expression of gp124, A15.5L, gp063, gp125, gp081, and gp066-based chimeras, we found a pronounced drop in pH, whereas, in the case of C20.5L and gp120, such  $H^+$  conduction was insignificant.

Based on the different quantitative channel activity assessments of the eight proteins, we ranked each between 1 and 8. Different color markings shown in Figure 4 describe the relative activity of the ion channel activity of the chimera. Based on the ranking for each chimera in the three bacterial assays, we calculated an average ranking for each system, and as an order of activity, they can be written in descending order as: A15.5L > gp081 > gp063 = gp120 > C20.5L > gp124 = gp125 > gp066. Finally, among these eight proteins, only the top five exhibited activity in the positive and negative bacterial assays. Therefore, these viral proteins can be considered potential channels worthy of further investigation by computational tools.

While the sequences of the above putative channels are known, alongside their activity in bacteria-based assay, their structural details are unavailable to us. Therefore, AlphaFold2-based structural predictions [29,39] were conducted to yield the proteins' putative structures. Since the proteins mostly likely form oligomers when functioning as channels, oligomers were constructed using AlphaFold2. Upon using both selection criteria (see Section 2.3.1), one structure was selected from each protein from several probable oligomeric structures depending upon the confidence value of the TM region (see Supplementary Figure S2). Finally, we did not obtain a suitable ion channel forming pore helical assembly for gp081.

The probable structures of the four ion channel proteins are depicted in Supplementary Figure S3. A central hollow core with concentric assembled  $\alpha$ -helices was found for all the structures. It is worth mentioning that AlphaFold2 is very effective in predicting



homo-oligomeric assembly [39]. Therefore, the assembled structural outputs, without lipid environments, show trimeric or tetrameric assembly with an arrangement of polar-hydrophobic-polar zones (Supplementary Figure S3), which is suitable for placing them within a triphasic lipid environment.

For C20.5L, gp063, and gp120, simple trimeric models were chosen (Supplementary Figure S3). For C20.5L, the segment-wise confidence level is more or less uniform in nature (Supplementary Figure S2). In the case of gp063, as evident from Supplementary Figures S2 and S3c, the confidence level of the less structured, charged, hydrophilic segments (with cyan protein segment) have relatively lower confidence, but the hydrophobic segments have much higher confidence (higher than 70%). On the other hand, for gp120, the overall level of confidence is lower. The probable TM segment has a value slightly higher than 50%.

Interestingly, the A15.5L structure exhibits different properties. The sequence of the monomeric protein segment has a discontinuous TM zone. From segments 25 to 29, there are two lysines and one aspartic acid residues. In the predicted AlphaFold2 structure, this hydrophilic segment has formed a turn, making two hydrophobic TM domains closer to each other, making a “V” shaped motif. From Supplementary Figure S3b, it can be seen that, upon oligomer formation, the arrangement has aligned it in a way so that the turn makes a charged end in the polar-hydrophobic-polar pattern. This makes the model suitable to fit within a lipid environment.

MD simulations were conducted to examine whether AlphaFold2 predicted if proteins are stable within the membrane environment. To this end, structures obtained from AlphaFold2 were embedded within a model 1,2-dipalmitoyl-sn-glycero-3-phosphocholine membrane for molecular dynamic simulation studies.

All four structures exhibit stability during the course of 100 ns within the lipid bilayer environment. Figure 5 shows the change in RMSD values for the backbone of each protein with respect to time. In all cases, the system converges during the course of the simulation. Finally, Figure 6 shows the structures of the four primary models of C20.5L, A15.5L, gp063, and gp120 placed within a lipid bilayer.

## 4. Materials and Methods

### 4.1. Searching Transmembrane Proteins

The genome of the MPVX virus (GenBank: ON563414.3) was analyzed for the presence of potential viroporins by searching every open reading frame for transmembrane helices using a hidden Markov model with TMHMM [43,44]. The same sequences were cross-checked with Phobius, another web-based model that checks transmembrane topology and signal peptide sequences [30,44]. Subsequently, all proteins with one or more predicted transmembrane helices were ranked according to size from smallest to largest, and the proteins smaller than 100 amino acids were selected for investigation: C20.5L, A15.5L, gp124, gp063, gp066, gp125, gp081 and gp120.

### 4.2. Bacterial Expression

For the channel assays, we expressed the genes of the aforementioned proteins within three types of *Escherichia coli* strains, namely, DH10B, LB650, and LR1. The DH10B strain was purchased from Invitrogen (Carlsbad, CA, USA). LB650, a K<sup>+</sup>-uptake deficient strain [35], was a kind gift from Professor K. Jung (Ludwig-Maximilians Universität München) and Professor G.A. Berkowitz (University of Connecticut). The LR1 strain for measuring H<sup>+</sup> flux [34] was a kind gift from Professor M. Willemoës and Professor K. Lindorff-Larsen (Københavns Universitet).

### 4.3. Plasmids

All the above-listed proteins were expressed in the corresponding cell lines as fusion proteins with the maltose binding protein employing the pMal-p2X vector (New England

Biolabs; Ipswich, MA, USA). The sequences were synthesized by GenScript (Piscataway, NJ, USA). In all cases, expressions were triggered by Isopropyl- $\beta$ -D-1-thiogalactopyranoside (IPTG).

#### 4.4. Chemicals

IPTG was purchased from Biochemika-Fluka (Buchs, Switzerland). All other chemicals were purchased from Sigma-Aldrich laboratories (Rehovot, Israel).

#### 4.5. Growth Media

Lysogeny Broth (LB) was used for all bacterial growth unless noted otherwise. LBK was similar to LB except that KCl replaces NaCl at 10 gr/L. All media contained ampicillin at 50  $\mu$ g/mL.

#### 4.6. Negative Ion Channel Assay

DH10B bacteria containing the desired plasmids were grown overnight, after which they were diluted 50 times and grown until the OD<sub>600nm</sub> reached a value of 0.2. From the culture, 50  $\mu$ L were added to 96-well plates containing 50  $\mu$ L of other required solutions. Induction of the desired proteins was achieved by adding IPTG at different concentrations. The bacterial growth kinetics were measured by monitoring the OD<sub>600nm</sub> of the resultant solutions using an infinite M200 pro (Tecan Group; Männedorf, Switzerland) or LogPhase 600 from BioTek (Santa Clara, CA, USA). The incubation time for each experiment was 16 h, and the experimental temperature was 37 °C with a shaking speed of 700 rpm. Every 15 min, data points were collected and plotted as a function of time.

#### 4.7. Positive Ion Channel Assay

A positive assay was conducted employing the same protocol as the negative ion channel assay listed above, except that LB50 bacteria, a K<sup>+</sup>-uptake deficient strain, was used [35]. Moreover, LBK media was used with 150 mM KCl instead of NaCl for overnight growth.

#### 4.8. Acidity Assay

This assay relies on the fluorescence of a pH-sensitive green fluorescent protein [38] present within the bacterial chromosome [34]. For this experiment, overnight bacterial cultures were diluted in a 1:50 ratio in LB media and further grown until the OD<sub>600nm</sub> reached 0.1. Proteins were expressed using IPTG at different concentrations. After one hour of induction, each of the cell growths was brought to an equivalent concentration of 0.2 OD<sub>600nm</sub> and was centrifuged at 2058  $\times$  g for 5 min. The pelleted cells were suspended in McILvaine Buffer [45] (200 mM Na<sub>2</sub>HPO<sub>4</sub> and 0.9% NaCl adjusted to pH 7.6 with 0.1 M citric acid). Subsequently, 200  $\mu$ L of this suspension was added to 96-well plates (Nunclon f96 Microwell Black Polystyrene, Thermo Fisher Scientific; Waltham, MA, USA), whereby each well contained 30  $\mu$ L of McILvaine Buffer. In the plate, three wells contained McILvaine buffer and three bacterial cultures without induction as control. The fluorescence data were measured with a microplate reader (Infinite F200 Pro, Tecan Group; Männedorf, Switzerland) at ambient temperature. Two fluorescence measurements were taken at each time point: 520 nm emission and either 390 nm or 466 nm excitation. At the starting point, 70  $\mu$ L of 300 mM citric acid was added to the bacteria culture, and fluorescence intensity data was measured for 120 s for each wavelength.

#### 4.9. Computational Studies

Primary protein sequences (oligomeric) were inputted into AlphaFold2.ipynb using ColabFold v1.5.2 to obtain tentative three-dimensional structures [39]. The outcome structures were subsequently embedded within a pre-equilibrated 1,2-dipalmitoyl-sn-glycero-3-phosphocholine bilayer downloaded from the website of D. Peter Tieleman [46] such that the protein helical axes remain perpendicular to the membrane plane. The bilayer had 128 lipid molecules and 3783 water molecules. After initial structural alignment, the clashing lipids and water molecules within the range of 2 Å were removed using In-

flateGro methodology developed by Tieleman and co-workers [47]. Position-restraints ( $100,000 \text{ kcal mol}^{-1} \text{ \AA}^{-2}$ ) on protein-heavy atoms were used to ensure that the protein does not change during energy minimization accomplished using the steepest descent minimization algorithm with a tolerance of  $500 \text{ kJ mol}^{-1} \text{ nm}^{-1}$ .

MD simulations for all the systems were conducted for a duration of 100 ns using Gromacs version 2022.3 [48–52] using an extended version of GROMOS96 53A6 force field [53]. The LINCS algorithm with an integration time step of 2 fs was used in all cases to constrain the length and angles of hydrogen atoms [54]. Atomic coordinates were saved at every 500 ps. Reference temperatures were set at 323 K, and solvent, lipids, and proteins were coupled separately to a Nose-Hoover temperature bath [55,56] with a coupling constant value  $\tau = 0.5 \text{ ps}$ . Pressure coupling was obtained with a Parrinello-Rahman barostat with  $\tau = 2 \text{ ps}$  [57,58]. A 1.2 nm cut-off was set for van der Waals interactions. The neighbor list was updated every 10 fs. Electrostatic parameters were calculated using fourth-order Particle Mesh Ewald (PME) long-range electrostatics [59], and cut-off short-range electrostatics were set to 1.2 nm.

The simulation box contained 125 lipid molecules and 3700 water molecules (the number varies as the size of the box changed for larger proteins), approximately with  $\text{Na}^+$  and  $\text{Cl}^-$  counter ions. Water molecules were fitted in the FLEXSPC model [60], and the total number of atoms was in the 17,000–25,000 range, depending on the protein sequence and oligomerization state. RMSD values with respect to time were extracted, and structures of the simulated proteins were visualized and analyzed with VMD software version 1.9.4a51 [61].

## 5. Conclusions

Potential Mpox viral ion channels were studied to assist future anti-viral drug discovery. Both experimental and computational studies were performed to characterize the activity of ion channels and to provide a preliminary idea of their tentative structural models. From three types of bacteria-based biochemical assays (negative, positive, and pH-flux), an average performance ranking was made, and out of eight proteins, five effective channels were obtained. These five sequences were inputted into AlphaFold2, an AI structure prediction approach, to determine each protein's tentative structure. These structures also showed good stability within the triphasic lipid environment upon MD simulation, and from an overlay of the converged structure, we proposed preliminary structures of four transmembrane ion channels of the Mpox virus. Finally, this study can potentially facilitate future progress in drug design against the Mpox virus.

**Supplementary Materials:** The following supporting information can be downloaded at: <https://www.mdpi.com/article/10.3390/ijms241813828/s1>.

**Author Contributions:** Conceptualization, K.B., M.K. and I.T.A.; methodology, K.B. and M.K.; software, K.B.; validation, K.B., M.K. and I.T.A.; formal analysis, K.B., M.K. and I.T.A.; investigation, K.B., M.K. and I.T.A.; resources, I.T.A.; data curation, K.B., M.K. and I.T.A.; writing—original draft preparation, K.B.; writing—review and editing, K.B. and I.T.A.; visualization, K.B., M.K. and I.T.A.; supervision, I.T.A.; project administration, I.T.A.; funding acquisition, I.T.A. All authors have read and agreed to the published version of the manuscript.

**Funding:** This research was funded in part by Israeli Science Foundation, grant number [948/19] and Israeli Science Ministry grant number [66257].

**Institutional Review Board Statement:** Not applicable.

**Informed Consent Statement:** Not applicable.

**Data Availability Statement:** All data are available upon request from the corresponding author.

**Conflicts of Interest:** The authors declare no conflict of interest.

## Abbreviations

The following abbreviations are used in this manuscript:

MPXV	Mpox or monkeypox virus
IPTG	Isopropyl- $\beta$ -D-1-thiogalactopyranoside
DPPC	1,2-dipalmitoyl-sn-glycero-3-phosphocholine
RMSD	Root mean square deviation

## References

- Lourie, B.; Bingham, P.G.; Evans, H.H.; Foster, S.O.; Nakano, J.H.; Herrmann, K.L. Human infection with monkeypox virus: Laboratory investigation of six cases in West Africa. *Bull. World Health Organ.* **1972**, *46*, 633–639. [[PubMed](#)]
- Antinori, A.; Mazzotta, V.; Vita, S.; Carletti, F.; Tacconi, D.; Lapini, L.E.; D'Abramo, A.; Cicalini, S.; Lapa, D.; Pittalis, S.; et al. Epidemiological, clinical and virological characteristics of four cases of monkeypox support transmission through sexual contact, Italy, May 2022. *Eurosurveillance* **2022**, *27*, 2200421. [[CrossRef](#)] [[PubMed](#)]
- Perez Duque, M.; Ribeiro, S.; Martins, J.V.; Casaca, P.; Leite, P.P.; Tavares, M.; Mansinho, K.; Duque, L.M.; Fernandes, C.; Cordeiro, R.; et al. Ongoing monkeypox virus outbreak, Portugal, 29 April to 23 May 2022. *Eurosurveillance* **2022**, *27*, 2200424. [[CrossRef](#)] [[PubMed](#)]
- Vivancos, R.; Anderson, C.; Blomquist, P.; Balasegaram, S.; Bell, A.; Bishop, L.; Brown, C.S.; Chow, Y.; Edeghere, O.; Florence, I.; et al. Community transmission of monkeypox in the United Kingdom, April to May 2022. *Eurosurveillance* **2022**, *27*, 2200422. [[CrossRef](#)] [[PubMed](#)]
- Gessain, A.; Nakoune, E.; Yazdanpanah, Y. Monkeypox. *N. Engl. J. Med.* **2022**, *387*, 1783–1793. [[CrossRef](#)] [[PubMed](#)]
- Shchelkunov, S.N.; Totmenin, A.V.; Safronov, P.F.; Mikheev, M.V.; Gutorov, V.V.; Ryazankina, O.I.; Petrov, N.A.; Babkin, I.V.; Uvarova, E.A.; Sandakhchiev, L.S.; et al. Analysis of the monkeypox virus genome. *Virology* **2002**, *297*, 172–194. [[CrossRef](#)]
- Kaler, J.; Hussain, A.; Flores, G.; Kheiri, S.; Desrosiers, D. Monkeypox: A Comprehensive Review of Transmission, Pathogenesis, and Manifestation. *Cureus* **2022**, *14*, e26531. [[CrossRef](#)]
- Laudisoit, A.; Tepage, F.; Colebunders, R. Oral Tecovirimat for the Treatment of Smallpox. *N. Engl. J. Med.* **2018**, *379*, 2084–2085. [[CrossRef](#)]
- Frenois-Veyrat, G.; Gallardo, F.; Gorgé, O.; Marcheteau, E.; Ferraris, O.; Baidaliuk, A.; Favier, A.L.; Enfroy, C.; Holy, X.; Lourenco, J.; et al. Tecovirimat is effective against human monkeypox virus in vitro at nanomolar concentrations. *Nat. Microbiol.* **2022**, *7*, 1951–1955. [[CrossRef](#)]
- Adler, H.; Gould, S.; Hine, P.; Snell, L.B.; Wong, W.; Houlihan, C.F.; Osborne, J.C.; Rampling, T.; Beadsworth, M.B.; Duncan, C.J.; et al. Clinical features and management of human monkeypox: A retrospective observational study in the UK. *Lancet Infect. Dis.* **2022**, *22*, 1153–1162. [[CrossRef](#)]
- Imran, M.; Alshammari, M.K.; Arora, M.K.; Dubey, A.K.; Das, S.S.; Kamal, M.; Alqahtani, A.S.A.; Sahloly, M.A.Y.; Alshammari, A.H.; Alhomam, H.M.; et al. Oral Brincidofovir Therapy for Monkeypox Outbreak: A Focused Review on the Therapeutic Potential, Clinical Studies, Patent Literature, and Prospects. *Biomedicines* **2023**, *11*, 278. [[CrossRef](#)] [[PubMed](#)]
- Scott, C.; Griffin, S. Viroporins: Structure, function and potential as antiviral targets. *J. Gen. Virol.* **2015**, *96*, 2000–2027. [[CrossRef](#)]
- Royle, J.; Dobson, S.J.; Müller, M.; Macdonald, A. Emerging Roles of Viroporins Encoded by DNA Viruses: Novel Targets for Antivirals? *Viruses* **2015**, *7*, 5375–5387. [[CrossRef](#)] [[PubMed](#)]
- To, J.; Surya, W.; Torres, J. Targeting the Channel Activity of Viroporins. *Adv. Protein Chem. Struct. Biol.* **2016**, *104*, 307–355. [[CrossRef](#)] [[PubMed](#)]
- Charlton, F.W.; Pearson, H.M.; Hover, S.; Lippiat, J.D.; Fontana, J.; Barr, J.N.; Mankouri, J. Ion channels as therapeutic targets for viral infections: Further discoveries and future perspectives. *Viruses* **2020**, *12*, 844. [[CrossRef](#)]
- Pinto, L.H.; Holsinger, L.J.; Lamb, R.A. Influenza virus M2 protein has ion channel activity. *Cell* **1992**, *69*, 517–528. [[CrossRef](#)]
- Davies, W.I.; Grunert, R.R.; Haff, R.F.; McGahen, J.W.; Neumayer, E.M.; Paulshock, M.; Watts, J.C.; Wood, T.R.; Hermann, E.C.; Hoffmann, C.E. Antiviral activity of 1-adamantanamine (amantadine). *Science* **1964**, *144*, 862–863. [[CrossRef](#)]
- Suzuki, T.; Orba, Y.; Okada, Y.; Sunden, Y.; Kimura, T.; Tanaka, S.; Nagashima, K.; Hall, W.W.; Sawa, H. The human polyoma JC virus agnoprotein acts as a viroporin. *PLoS Pathog.* **2010**, *6*, e1000801. [[CrossRef](#)]
- Suzuki, T.; Orba, Y.; Makino, Y.; Okada, Y.; Sunden, Y.; Hasegawa, H.; Hall, W.W.; Sawa, H. Viroporin activity of the JC polyomavirus is regulated by interactions with the adaptor protein complex 3. *Proc. Natl. Acad. Sci. USA* **2013**, *110*, 18668–18673. [[CrossRef](#)]
- Coric, P.; Saribas, A.S.; Abou-Gharbia, M.; Childers, W.; White, M.K.; Bouaziz, S.; Safak, M. Nuclear magnetic resonance structure revealed that the human polyomavirus JC virus agnoprotein contains an  $\alpha$ -helix encompassing the Leu/Ile/Phe-rich domain. *J. Virol.* **2014**, *88*, 6556–6575. [[CrossRef](#)]
- Tomar, P.P.S.; Krugliak, M.; Arkin, I.T. Blockers of the SARS-CoV-2 3a Channel Identified by Targeted Drug Repurposing. *Viruses* **2021**, *13*, 532. [[CrossRef](#)] [[PubMed](#)]
- Lahiri, H.; Arkin, I.T. Searching for blockers of dengue and West Nile virus Viroporins. *Viruses* **2022**, *14*, 1750. [[CrossRef](#)] [[PubMed](#)]



23. Tomar, P.P.S.; Arkin, I.T. SARS-CoV-2 E protein is a potential ion channel that can be inhibited by Gliclazide and Memantine. *Biochem. Biophys. Res. Commun.* **2020**, *530*, 10–14. [[CrossRef](#)]
24. Tomar, P.P.S.; Oren, R.; Krugliak, M.; Arkin, I.T. Potential viroporin candidates from pathogenic viruses using bacteria-based bioassays. *Viruses* **2019**, *11*, 632. [[CrossRef](#)]
25. Petersen, B.W.; Damon, I.K.; Bennett, J.; Dolin, R.; Blaser, M. Orthopoxviruses: Vaccinia (smallpox vaccine), variola (smallpox), monkeypox, and cowpox. In *Mandell, Douglas, and Bennett's Principles and Practice of Infectious Diseases*, 8th ed.; Elsevier: Philadelphia, PA, USA, 2014.
26. Bar-On, Y.M.; Flamholz, A.; Phillips, R.; Milo, R. SARS-CoV-2 (COVID-19) by the numbers. *Elife* **2020**, *9*, e57309. [[CrossRef](#)]
27. Lansiaux, E.; Jain, N.; Laivacuma, S.; Reinis, A. The virology of human monkeypox virus (hMPXV): A brief overview. *Virus Res.* **2022**, *322*, 198932. [[CrossRef](#)] [[PubMed](#)]
28. Kugelman, J.R.; Johnston, S.C.; Mulembakani, P.M.; Kitalu, N.; Lee, M.S.; Koroleva, G.; McCarthy, S.E.; Gestole, M.C.; Wolfe, N.D.; Fair, J.N.; et al. Genomic variability of monkeypox virus among humans, Democratic Republic of the Congo. *Emerg. Infect. Dis.* **2014**, *20*, 232–239. [[CrossRef](#)]
29. Jumper, J.; Evans, R.; Pritzel, A.; Green, T.; Figurnov, M.; Ronneberger, O.; Tunyasuvunakool, K.; Bates, R.; Židek, A.; Potapenko, A.; et al. Highly accurate protein structure prediction with AlphaFold. *Nature* **2021**, *596*, 583–589. [[CrossRef](#)]
30. Käll, L.; Krogh, A.; Sonnhammer, E.L. Advantages of combined transmembrane topology and signal peptide prediction—The Phobius web server. *Nucleic Acids Res.* **2007**, *35*, W429–W432. [[CrossRef](#)]
31. Hallgren, J.; Tsigirigos, K.D.; Pedersen, M.D.; Almagro Armenteros, J.J.; Marcatili, P.; Nielsen, H.; Krogh, A.; Winther, O. DeepTMHMM predicts alpha and beta transmembrane proteins using deep neural networks. *bioRxiv* **2022**. [[CrossRef](#)]
32. Tomar, P.P.S.; Krugliak, M.; Arkin, I.T. Identification of SARS-CoV-2 E Channel Blockers from a Repurposed Drug Library. *Pharmaceuticals* **2021**, *14*, 604. [[CrossRef](#)] [[PubMed](#)]
33. Astrahan, P.; Flitman-Tene, R.; Bennett, E.R.; Krugliak, M.; Gilon, C.; Arkin, I.T. Quantitative analysis of influenza M2 channel blockers. *Biochim. Biophys. Acta* **2011**, *1808*, 394–398. [[CrossRef](#)] [[PubMed](#)]
34. Santner, P.; Martins, J.M.d.S.; Laursen, J.S.; Behrendt, L.; Riber, L.; Olsen, C.A.; Arkin, I.T.; Winther, J.R.; Willemoës, M.; Lindorff-Larsen, K. A Robust Proton Flux (pHlux) Assay for Studying the Function and Inhibition of the Influenza A M2 Proton Channel. *Biochemistry* **2018**, *57*, 5949–5956. [[CrossRef](#)] [[PubMed](#)]
35. Stumpe, S.; Bakker, E.P. Requirement of a Large K<sup>+</sup>-Uptake Capacity and of Extracytoplasmic Protease Activity for Protamine Resistance of *Escherichia Coli*. *Arch. Microbiol.* **1997**, *167*, 126–136. [[CrossRef](#)]
36. Taube, R.; Alhadeff, R.; Assa, D.; Krugliak, M.; Arkin, I.T. Bacteria-based analysis of HIV-1 Vpu channel activity. *PLoS ONE* **2014**, *9*, e105387. [[CrossRef](#)]
37. Assa, D.; Alhadeff, R.; Krugliak, M.; Arkin, I.T. Mapping the Resistance Potential of Influenza's H<sup>+</sup> Channel against an Antiviral Blocker. *J. Mol. Biol.* **2016**, *428*, 4209–4217. [[CrossRef](#)]
38. Miesenböck, G.; De Angelis, D.A.; Rothman, J.E. Visualizing secretion and synaptic transmission with pH-sensitive green fluorescent proteins. *Nature* **1998**, *394*, 192–195. [[CrossRef](#)]
39. Mirdita, M.; Schütze, K.; Moriawaki, Y.; Heo, L.; Ovchinnikov, S.; Steinegger, M. ColabFold: Making protein folding accessible to all. *Nat. Methods* **2022**, *19*, 679–682. [[CrossRef](#)]
40. Hegedűs, T.; Geisler, M.; Lukács, G.L.; Farkas, B. Ins and outs of AlphaFold2 transmembrane protein structure predictions. *Cell. Mol. Life Sci.* **2022**, *79*, 73. [[CrossRef](#)]
41. Gonzalez, M.E.; Carrasco, L. Viroporins. *FEBS Lett.* **2003**, *552*, 28–34. [[CrossRef](#)]
42. David, A.; Islam, S.; Tankhilevich, E.; Sternberg, M.J. The AlphaFold database of protein structures: A biologist's guide. *J. Mol. Biol.* **2022**, *434*, 167336. [[CrossRef](#)] [[PubMed](#)]
43. Krogh, A.; Larsson, B.; von Heijne, G.; Sonnhammer, E.L. Predicting Transmembrane Protein Topology With a Hidden Markov Model: Application to Complete Genomes. *J. Mol. Biol.* **2001**, *305*, 567–580. [[CrossRef](#)] [[PubMed](#)]
44. Sonnhammer, E.L.; von Heijne, G.; Krogh, A. A Hidden Markov Model for Predicting Transmembrane Helices in Protein Sequences. *Proc. Int. Conf. Intell. Syst. Mol. Biol.* **1998**, *6*, 175–182.
45. McIlvaine, T. A Buffer Solution for Colorimetric Comparison. *J. Biol. Chem.* **1921**, *49*, 183–186. [[CrossRef](#)]
46. Berger, O.; Edholm, O.; Jähnig, F. Molecular dynamics simulations of a fluid bilayer of dipalmitoylphosphatidylcholine at full hydration, constant pressure, and constant temperature. *Biophys. J.* **1997**, *72*, 2002–2013. [[CrossRef](#)] [[PubMed](#)]
47. Kandt, C.; Ash, W.L.; Tieleman, D.P. Setting up and running molecular dynamics simulations of membrane proteins. *Methods* **2007**, *41*, 475–488. [[CrossRef](#)]
48. Abraham, M.J.; Murtola, T.; Schulz, R.; Páll, S.; Smith, J.C.; Hess, B.; Lindahl, E. GROMACS: High performance molecular simulations through multi-level parallelism from laptops to supercomputers. *SoftwareX* **2015**, *1*, 19–25. [[CrossRef](#)]
49. Bekker, H.; Berendsen, H.; Dijkstra, E.; Achterop, S.; Vondrumen, R.; Vanderspoel, D.; Sijbers, A.; Keegstra, H.; Renardus, M. Gromacs—A parallel computer for molecular-dynamics simulations. In *Proceedings of the 4th International Conference on Computational Physics (PC 92)*, Prague, Czech Republic, 24–28 August 1992; World Scientific Publishing: Singapore, 1993; pp. 252–256.
50. Berendsen, H.J.; van der Spoel, D.; van Drunen, R. GROMACS: A message-passing parallel molecular dynamics implementation. *Comput. Phys. Commun.* **1995**, *91*, 43–56. [[CrossRef](#)]

51. Lindahl, E.; Hess, B.; Van Der Spoel, D. GROMACS 3.0: A package for molecular simulation and trajectory analysis. *Mol. Model. Annu.* **2001**, *7*, 306–317. [[CrossRef](#)]
52. Pronk, S.; Páll, S.; Schulz, R.; Larsson, P.; Bjelkmar, P.; Apostolov, R.; Shirts, M.R.; Smith, J.C.; Kasson, P.M.; Van Der Spoel, D.; et al. GROMACS 4.5: A high-throughput and highly parallel open source molecular simulation toolkit. *Bioinformatics* **2013**, *29*, 845–854. [[CrossRef](#)]
53. Oostenbrink, C.; Villa, A.; Mark, A.E.; Van Gunsteren, W.F. A biomolecular force field based on the free enthalpy of hydration and solvation: The GROMOS force-field parameter sets 53A5 and 53A6. *J. Comput. Chem.* **2004**, *25*, 1656–1676. [[CrossRef](#)] [[PubMed](#)]
54. Hess, B.; Bekker, H.; Berendsen, H.J.; Fraaije, J.G. LINCS: A linear constraint solver for molecular simulations. *J. Comput. Chem.* **1997**, *18*, 1463–1472. [[CrossRef](#)]
55. Nosé, S. A molecular dynamics method for simulations in the canonical ensemble. *Mol. Phys.* **1984**, *52*, 255–268. [[CrossRef](#)]
56. Hoover, W.G. Canonical dynamics: Equilibrium phase-space distributions. *Phys. Rev. A* **1985**, *31*, 1695. [[CrossRef](#)] [[PubMed](#)]
57. Parrinello, M.; Rahman, A. Polymorphic transitions in single crystals: A new molecular dynamics method. *J. Appl. Phys.* **1981**, *52*, 7182–7190. [[CrossRef](#)]
58. Nosé, S.; Klein, M. Constant pressure molecular dynamics for molecular systems. *Mol. Phys.* **1983**, *50*, 1055–1076. [[CrossRef](#)]
59. Darden, T.; York, D.; Pedersen, L. Particle mesh Ewald: An  $N \cdot \log(N)$  method for Ewald sums in large systems. *J. Chem. Phys.* **1993**, *98*, 10089–10092. [[CrossRef](#)]
60. Berendsen, H.J.; Grigera, J.R.; Straatsma, T.P. The missing term in effective pair potentials. *J. Phys. Chem.* **1987**, *91*, 6269–6271. [[CrossRef](#)]
61. Humphrey, W.; Dalke, A.; Schulten, K. VMD: Visual molecular dynamics. *J. Mol. Graph.* **1996**, *14*, 33–38. [[CrossRef](#)]

**Disclaimer/Publisher’s Note:** The statements, opinions and data contained in all publications are solely those of the individual author(s) and contributor(s) and not of MDPI and/or the editor(s). MDPI and/or the editor(s) disclaim responsibility for any injury to people or property resulting from any ideas, methods, instructions or products referred to in the content.